Chaos, Solitons and Fractals 200 (2025) 117014

Contents lists available at ScienceDirect

Chaos, Solitons and Fractals

journal homepage: www.elsevier.com/locate/chaos

Dynamical modeling of hippocampal-basal ganglia interactions for spatial navigation

Haobin Wei [a], Lining Yin [a], Songan Hou [a], Ying Yu [a,*], Qingyun Wang [a,b]

[a] Department of Dynamics and Control, Beihang University, Beijing, 100191, China
[b] Ningxia Basic Science Research Center of Mathematics, Ningxia University, Yinchuan 750021, China

ARTICLE INFO

Keywords:
Hippocampal-basal ganglia circuit
Navigation
Spike-timing-dependent plasticity
Biologically inspired model
Neural dynamics

ABSTRACT

Coordinated interactions between the hippocampus and basal ganglia are known to support navigational decision-making, yet their precise collaborative mechanisms remain elusive. Based on biological theories, this study establishes a hippocampal-basal ganglia circuit model for navigation. Unlike existing neural reinforcement learning models, the proposed model aims to investigate how the interaction between the hippocampus and basal ganglia influences navigation. The model incorporates spike-timing-dependent plasticity (STDP) and dopamine-mediated reinforcement learning, enabling the hippocampal module to learn environments and retain goal memories in an allocentric (world-centered) coordinate system. Additionally, it integrates a cortico-basal ganglia network to address choice conflicts. This network receives egocentric (self-centered) landmark inputs and establishes stimulus-action associations through synaptic plasticity. By combining the hippocampus's spatial representation and the basal ganglia's action selection strategy, the model simulates the decision-making process from spatial learning to motor execution. Furthermore, the model successfully reproduces rodent navigation behaviors in Morris water maze and plus maze paradigms, demonstrating lesion-induced deficits matching biological observations. Finally, validation through mobile robot navigation task confirms physical realizability. The model demonstrates biological plausibility, mechanistically explaining how action sequences are generated during biological navigation. It provides a novel computational perspective for understanding the neural basis of navigational behavior.

1. Introduction

To ensure survival in competitive natural environments, animals are required to develop efficient strategies for achieving goal-oriented navigation. Numerous species, particularly rodents and chiropterans [1,2], demonstrate remarkable adaptive flexibility in navigation. These behavioral capabilities, along with their underlying neural mechanisms, are widely used as core reference paradigms for the bionic design of mobile robots [3,4]. Consequently, elucidating the neural substrates of animal navigation has emerged as a prominent research direction in neuromorphic navigation studies.

Current studies distinguish two principal navigation learning modalities: "place learning" and "response learning", with well-documented behavioral and neural differences [5–7]. "Place learning" facilitates the formation of flexible cognitive representations of spatial configurations [8–10], conceptually aligned with Tolman's cognitive map hypothesis [11]. This allocentric strategy is predominantly hippocampus-dependent. In contrast, "response learning" establishes stimulus–response associations that underlie

* Corresponding author.
E-mail address: yuyingmath@163.com (Y. Yu).

https://doi.org/10.1016/j.chaos.2025.117014
Received 5 June 2025; Received in revised form 25 July 2025; Accepted 4 August 2025
Available online 15 August 2025

habitual navigation behaviors, mediated primarily by the dorsolateral striatum within the basal ganglia circuitry [12,13]. These distinct neural systems operate synergistically to support complex navigation behaviors.

Extensive research has demonstrated that the hippocampus plays a crucial role in navigation. Hippocampal cells possess spatial selectivity and spatial memory, serving as the neural foundation for cognitive map formation [14,15]. Subsequent experimental research has revealed their predictive coding properties: place cell ensembles exhibit preplay and replay of future trajectories [16,17], while CA1 neuronal activity accurately predicts imminent spatial positions [18], suggesting their role in prospective behavioral guidance. From a computational perspective, Stachenfeld et al. [19] demonstrated that the successor representation (SR) framework effectively models place cells' predictive coding characteristics, reward sensitivity, and policy dependence. Moreover, Bono et al. [20] developed a biophysically constrained CA3-CA1 network model that implements SR-like predictive map learning through biologically plausible synaptic plasticity mechanisms. Meanwhile, extensive research has focused on hippocampal navigation models. For instance, Yan et al. developed a three-layer feedforward network incorporating the hippocampus, successfully reconstructing the firing fields of both place cells and grid cells while achieving navigation functionality [21]. Luca et al. introduced a system within multiple grid-cell modules for self-position estimation in a mobile robot, and demonstrated that coordinated neuronal firing in the hippocampus enhances the accuracy and reliability of spatial navigation [22].

In contrast to the hippocampus's spatial mapping functions, the striatum within the basal ganglia supports procedural learning through reinforcement mechanisms mediated by dopamine [23,24]. The distinct method aims to associate actions with sensory inputs, forming "habitual" stimulus-driven movements [25]. By applying a cortico-striatal circuit model, Chersi et al. [26] successfully simulated the transition between goal-directed and habitual control during associative remapping tasks. Such behavioral switching has been observed in spatial navigation paradigms [27,28].

Recent computational models have attempted to integrate these complementary systems to better capture navigation flexibility. Sukumar et al. [29] proposed a competitive hippocampal-striatal model that accounted for behavioral strategy shifts in Morris water maze navigation through interactions between cue module and place module. Similarly, Geerts et al. [30] developed a reinforcement learning framework that captured navigation strategy transitions between model-based (hippocampal) and model-free (striatal) systems while preserving the SR formalism for spatial learning. However, these models often rely on machine learning and lack biological plausibility. Although recent studies have employed spiking neural networks (SNNs) to model navigation behaviors [31,32], they remain poorly incorporate detailed hippocampal-basal ganglia microcircuitry and their associated learning rules.

In this study, we present a biologically constrained spiking neural network model consists of hippocampal and basal ganglia microcircuits. The proposed model incorporates spike-timing-dependent plasticity (STDP) and reward-modulated STDP (R-STDP) to mediate learning. The hippocampal module encodes allocentric spatial representations through cortico-hippocampal and intra-hippocampal synaptic plasticity, while the basal ganglia module generates action sequences via cortico-striatal reinforcement learning. This integrated architecture successfully replicates both normal and lesion-induced behavioral phenotypes in mice during Morris water maze and plus maze navigation tasks. Finally, our model is applied to control a mobile robot in a navigation task to validate the physical realizability. By addressing the limitations of existing SNN and RL models—particularly the lack of biologically grounded inter-region coordination—our framework offers novel insights into the neural mechanisms of navigation and adaptive behavior.

2. Model and method

2.1. Model architecture

We propose a hippocampal-basal ganglia circuits model for spatial navigation, as illustrated in Fig. 1. The model consists of two components: the hippocampus and the cortico-basal ganglia loop, each generating distinct navigation strategies based on different input information.

The cortico-basal ganglia circuit is modeled as a network comprising landmark cells (LCs) in the sensorimotor cortex [30,33], motor cortex (MC), inhibitory neuron (INH), substantia nigra pars reticulata (SNr), thalamus (TH), and basal ganglia (BG). The neuron number for each component is listed in Table 1, and their synaptic connections are detailed in Table 2.

The LCs consist of a 15×15 neuronal pool, with each neuron encoding a preferred landmark position in egocentric coordinates. For instance, when a landmark is located 5 m ahead of the agent, the neuron encoding the "5 m ahead" position fires at 30 Hz while other LC neurons remain silent. As the primary input nucleus to the BG, the LCs form plastic connections with the striatum that are modulated during learning.

The basal ganglia are further subdivided into striatal D1 (D1), striatal D2 (D2), subthalamic nucleus (STN), and globus pallidus externa (GPe). The D1 and D2 striatal neurons, distinguished by their dopamine receptor types, serve as the basal ganglia's main input nuclei receiving inputs from both LCs and MC. The D1 striatum mediates the direct pathway (D1-SNr-TH), while the D2 striatum mediates the indirect pathway (D2-GPe-SNr-TH) (Fig. 1). The direct pathway facilitates action selection, whereas the indirect pathway suppresses it. The SNr, as the BG output nucleus, provides inhibitory projections to TH. Action selection is mediated by TH disinhibition, where the coordinated activity of both direct and indirect pathways for a particular action suppresses SNr activity, ultimately resulting in disinhibition of the corresponding TH. The enhanced TH activity then influences the associated MC neuron through the circuit, with MC activation marking action selection. Our model incorporated N distinct action channels, each corresponding to a different movement alternative. These channels are anatomically segregated within the basal ganglia but

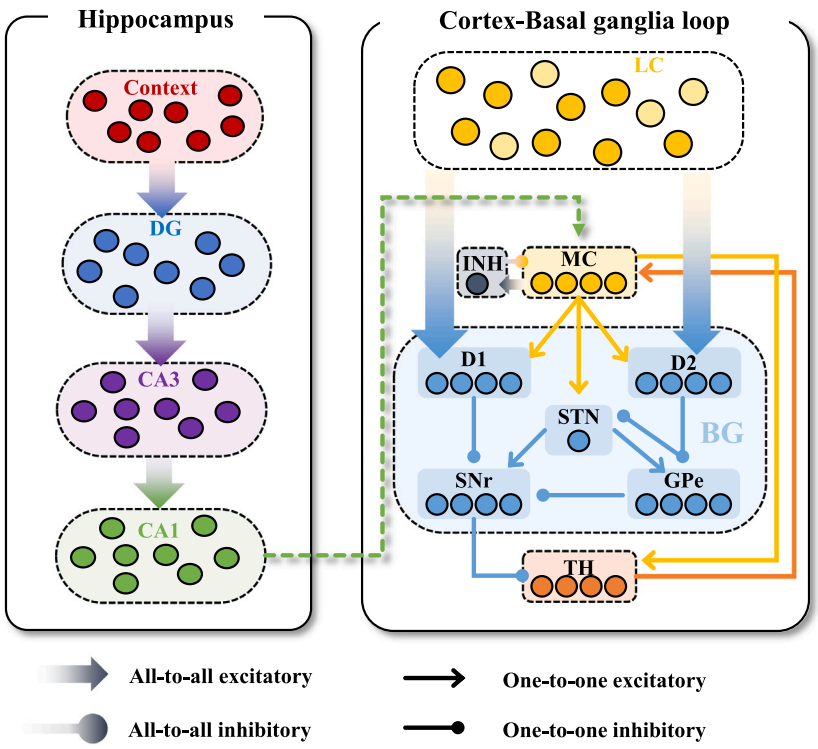

Fig. 1. Scheme of the network model. The connections of LC-BG, DG-CA3, CA3-CA1, as well as context-DG are plastic. The dashed connections in figure stand for functional inputs from CA1 to the MC. The LC receives input and encodes landmark location in egocentric system while DG, CA3 and CA1 encode self-position in allocentric system. The motor cortex controls agent movements. Abbreviations: DG, dentate gyrus; LC landmark cell; MC, motor cortex; INH, inhibitory neuron; D1, striatumD1; D2, striatumD2; STN, subthalamic nucleus; GPe, globus pallidus pars externa; SNr, substantia nigra pars reticulata; TH, thalamus. Thick gray arrows indicate all-to-all excitatory connections, while gray arrows with filled circles represent all-to-all inhibitory connections. Thin black arrows and black arrows with filled circles denote one-to-one excitatory and inhibitory connections, respectively.

Table 1
Number of neurons in each component of the navigation model.

	Neuron layer	Number
Cortical-basal ganglia loop	D1	8
	D2	8
	SNr	8
	GPe	8
	STN	1
	INH	1
	MC	8
	TH	8
	LC	225
Hippocampus	Context	4
	DG	225
	CA3	225
	CA1	225

achieve competitive selection via a biologically inspired winner-take-all (WTA) mechanism. Specifically, MC neurons establish all-to-all excitatory projections to a shared pool of inhibitory interneurons, which in turn send uniform inhibitory feedback to the entire MC population. This lateral inhibition architecture enables only one action channel to dominate at a time through dynamic network competition, effectively implementing mutual suppression among competing motor outputs [34].

The STN constitutes another major input nucleus to the BG, receiving cortical inputs. Animal studies demonstrate that STN lesions impair response selection and cause premature choices when conflict resolution requires competitive inhibition [35,36]. Following Baston's modeling approach for the hyper-direct pathway mediated by STN [34], our model employs the STN for conflict monitoring. Simultaneous activation of multiple MC neurons indicates conflict and triggers abnormal STN activity. As shown in Fig. 1, this activity provides diffuse excitatory input to SNr and GPe, thereby suppressing weaker activations in competing MC neurons

Table 2
Neuronal connectivity in the hippocampal-basal ganglia model.

	Neuron		Synaptic	
One-to-one connection	Pre	Post	Type	Number
	MC	D1	Excitatory	8
	MC	D2	Excitatory	8
	D1	SNr	Inhibitory	8
	D2	GPe	Inhibitory	8
	GPe	SNr	Inhibitory	8
	SNr	TH	Inhibitory	8
	TH	MC	Excitatory	8
	MC	TH	Excitatory	8
All-to-all connection	MC	STN	Excitatory	8
	MC	INH	Excitatory	8
	INH	MC	Inhibitory	8
	STN	GPe	Excitatory	8
	STN	SNr	Excitatory	8
	LC	D1	Excitatory	1800
	LC	D2	Excitatory	1800
	Context	DG	Excitatory	900
	DG	CA3	Excitatory	50 625
	CA3	CA1	Excitatory	50 625

and ultimately reducing conflict probability. Additionally, the MC neurons follow a winner-take-all (WTA) principle, where the network's excitatory–inhibitory connectivity ensures only one MC neuron exhibits high-frequency firing at any time, representing a single selected action, which in this task corresponds to the agent's movement direction. The combined action of STN conflict monitoring and WTA circuitry guarantees unique action selection per decision.

The hippocampal model comprises dentate gyrus (DG), CA3, and CA1 neurons, each implemented as a 15×15 neuronal pool. DG, CA3, and CA1 all encode the agent's global position in allocentric coordinates, with neuronal firing rates correlating with spatial location — neurons corresponding to the agent's current allocentric position show high-frequency firing. To assess the impact of spatial resolution, we also test alternative grid sizes (e.g., 10×10 and 20×20), and find that task performance remains comparable. Thus, the 15×15 configuration is selected as a compromise between spatial precision and computational efficiency.

The DG additionally receives contextual input from the cortex, where context neurons encoding the agent's goal-seeking intention maintain sustained activity throughout the task [37,38]. CA3 receives excitatory input from DG, while CA1 receives excitatory input from CA3. The hippocampal anatomical structure is referenced from Amaral and Lavenex [39]. Detailed connectivity patterns are provided in Table 2, with specific learning rules discussed in Section 2.3.

2.2. Neuron model

In this study, all neuronal models employ the leaky integrate-and-fire (LIF) framework. The subthreshold membrane potential is described by:

$$\tau_{\mathrm{m}} \frac{dV(t)}{dt} = -(V(t) - V_{\mathrm{L}}) + R_{\mathrm{m}} \cdot I_{\mathrm{syn}}(t) \tag{1}$$

where $V_{\mathrm{L}} = -70$ mV represents the resting potential, R_{m} denotes the membrane resistance, and τ_{m} indicates the membrane time constant.

When the membrane potential reaches the threshold potential $V_{\mathrm{th}} = -55$ mV, the neuron generates an action potential and subsequently resets to $V_{\mathrm{L}} = -70$ mV. For all neurons in our model, $R_{\mathrm{m}} = 33$ MΩ and $\tau_{\mathrm{m}} = 33$ ms.

The total synaptic current $I_{\mathrm{syn}}(t)$ at time t is given by:

$$I_{\mathrm{syn}}(t) = I_{\mathrm{AMPA}}(t) + I_{\mathrm{GABA}}(t) \tag{2}$$

This synaptic current comprises both glutamatergic excitatory (AMPA) and GABA inhibitory components. For each receptor type X, including AMPA and GABA receptors, the corresponding current follows:

$$I_X(t) = g_X \cdot (V(t) - E_X) \tag{3}$$

$$\frac{dg_X}{dt} = -\frac{g_X}{\tau_X} + \bar{g}_X \cdot W \cdot \sum_{t^{(f)}} \delta(t - t^{(f)}) \tag{4}$$

Here, $V(t)$ represents the postsynaptic membrane potential, E_X denotes the reversal potential, and g_X indicates the synaptic conductance. The conductance dynamics obey Eq. (4), where τ_X is the time constant, $\bar{g}_X$ represents the conductance increment, and $t^{(f)}$ denotes the presynaptic spike train. When a presynaptic spike occurs, the conductance instantaneously increases by $\bar{g}_X$. W signifies the synaptic strength, which undergoes modification during learning for plastic synapses, while non-plastic synapses maintain a fixed strength of $W = 1$ throughout simulations. Eqs. (3) and (4) can capture the nonlinear interaction between membrane

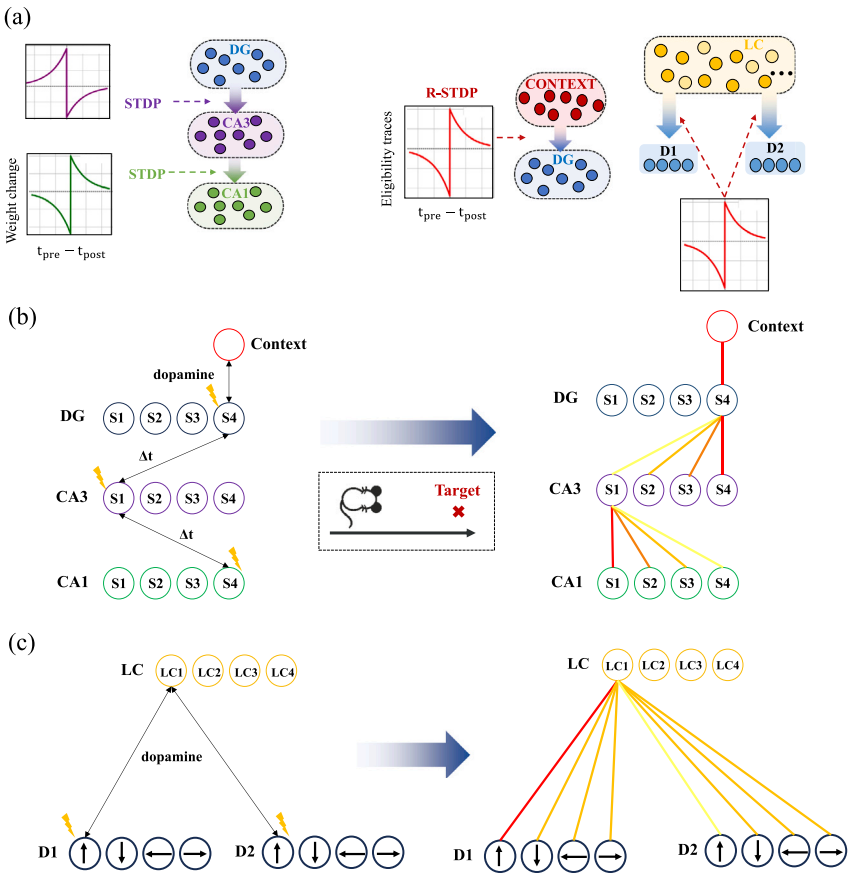

Fig. 2. Schematic diagram of learning rules. (a) Plastic synaptic connections and their corresponding learning rules in the basal ganglia module. (b) An example of learning in the hippocampal module. The line color gradient from dark to light (red to yellow) represents the corresponding variation in synaptic weights from strong to weak. (c) An example of learning in the basal ganglia module. (For interpretation of the references to color in this figure legend, the reader is referred to the web version of this article.)

potential and conductance, which reflects realistic postsynaptic integration, particularly in bio-physically inspired spiking networks. For AMPA synapse $E_{\mathrm{AMPA}} = 0$ mV, $g_{\mathrm{AMPA}} = 8 \times 10^{-5}$ mS, $\tau_{\mathrm{AMPA}} = 10$ ms, and for GABA synapse $E_{\mathrm{GABA}} = -90$ mV, $g_{\mathrm{GABA}} = 7 \times 10^{-5}$ mS, $\tau_{\mathrm{GABA}} = 10$ ms.

2.3. Learning rule

In our model, the synaptic weights are updated across multiple neural connections including LC-BG, DG-CA3, CA3-CA1, and context-DG.

The synaptic weights of DG-CA3 and CA3-CA1 connections are updated in real-time according to the STDP rule:

$$\Delta W(\Delta t) = \begin{cases} A_+ \cdot \exp(-\Delta t/\tau_+) & \text{if } \Delta t > 0 \\ A_- \cdot \exp(\Delta t/\tau_-) & \text{if } \Delta t < 0, \end{cases} \tag{5}$$

$$\tau_{\mathrm{w}} \frac{dW}{dt} = -W + \Delta W \tag{6}$$

where Δt represents the spike-timing difference between presynaptic and postsynaptic neurons, A_+ and A_- determine the maximum weight adjustment values, τ_+ and τ_- define the temporal window for synaptic modification. Parameter values for these two synaptic pathways are listed in Table 3 [40].

Following Jacopo et al.'s hippocampal modeling framework [20], our implementation incorporates location-dependent current inputs to DG, CA3, and CA1 regions, which are physiologically modeled as originating from the entorhinal cortex. The learning mechanism operates through STDP, where synaptic weights are modified according to precise temporal relationships between pre- and postsynaptic spikes, forming environmental spatial representations. Unlike classic STDP models constrained to sub-100 ms plasticity windows, we adopt longer time constants (e.g., $\tau_- = 4000$ ms for DG–CA3) to support temporally extended associations. This setting is used to integrate spatial context over longer trajectories. For example, during navigation, DG neurons encoding

Table 3
Parameter values of the STDP learning rule in the hippocampus.

Parameter	DG-CA3	CA3-CA1
A_+	0.1	−0.1
A_-	−0.1	0.1
τ_+	50 ms	30 ms
τ_-	4000 ms	30 ms
τ_W	10 s	10 s

the target context fire early, while CA3 neurons activate sequentially along the path. The long STDP window enables synaptic potentiation between DG and multiple downstream CA3 neurons at varying delays, with weights scaled by the time difference. Such an approach supports distributed memory traces spanning across positions, consistent with theoretical models of sequence learning and trajectory association [41]. As illustrated in Fig. 2(b), we simulate an agent performing constant-velocity navigation from position S1 to target position S4, which generated sequential activation patterns (S1→S2→S3→S4) across DG, CA3, and CA1 neuronal populations. The plastic DG-CA3 connections developed weight patterns reflecting spatial proximity, with the $S4_{DG}$→$S1_{CA3}$ connection showing minimal potentiation due to the longest spike interval (corresponding to maximal spatial distance), while the $S4_{DG}$→$S4_{CA3}$ connection exhibited maximal potentiation. Simultaneously, the CA3-CA1 connections encoded transition probabilities between locations. The $S1_{CA3}$→$S1_{CA1}$ connection demonstrated the strongest potentiation, indicating minimal transition cost when remaining at the same position, whereas the $S1_{CA3}$→$S4_{CA1}$ connection showed the weakest potentiation, representing the most costly transition. These differential synaptic modifications collectively enable the system to learn both spatial relationships and navigation costs within the environment.

To support temporally delayed reward learning consistent with dopaminergic plasticity, we adopt a reward-modulated STDP framework incorporating eligibility traces as proposed in Izhikevich [42]. In our model, the synaptic weights between contextual neurons and the DG neuronal layer are not updated instantaneously but rather modified through R-STDP. We introduce a variable $F(\Delta t)$ is used to represent the dependence of synaptic weight changes on historical neuronal activity, described as:

$$F(\Delta t) = \begin{cases} A_+ \cdot \exp(-\Delta t/\tau_+) & \text{if } \Delta t > 0 \\ A_- \cdot \exp(\Delta t/\tau-) & \text{if } \Delta t < 0 \end{cases} \tag{7}$$

where F influences the evolution of eligibility traces, ultimately modifying synaptic weights according to:

$$\tau_E \frac{dE}{dt} = -E + F(\Delta t) \tag{8}$$

$$\tau_w \frac{dW}{dt} = -W + R \cdot E + H \cdot E \tag{9}$$

Here, E represents the eligibility trace of co-activation between pre- and postsynaptic neurons τ_E denotes the decay time constant of eligibility traces. This design allows the model to solve the classical distal reward problem by preserving a decaying memory trace of recent state–action activations at synapses. Upon delayed reward arrival, these traces are converted into actual synaptic changes based on their temporal proximity to the reward signal. The model parameters are modified from Izhikevich [42] and Florian [43].

Synaptic updates are modulated by two neuromodulators: dopamine R, which exhibits rapid phasic elevation upon successful reward discovery, and acetylcholine H, which shows transient increases during exploration phases without reward. Dopamine amplifies synaptic potentiation when eligibility traces align with rewarded outcomes, while acetylcholine promotes plasticity during non-rewarded decision-making phases, enhancing future learning. This dual neuromodulation mechanism is inspired by Zannone et al. [31], which demonstrate that acetylcholine modulates synaptic sensitivity during unrewarded learning phases, while dopamine consolidates synaptic modifications upon successful reward acquisition. This cooperative modulation mechanism has also been supported by recent neurophysiological findings in rodents, suggesting complementary roles of acetylcholine and dopamine in guiding learning and navigation under uncertainty [44]. The dopamine concentration R and acetylcholine concentration H are modeled as:

$$\tau_R \frac{dR}{dt} = -R + DA(t) \tag{10}$$

$$\tau_H \frac{dH}{dt} = -H + AC(t) \tag{11}$$

$$DA(t) = \begin{cases} 0.01 & t = t_{reward} \\ 0 & \text{otherwise} \end{cases} \tag{12}$$

$$AC(t) = \begin{cases} 0.0005 & t = t_{no} \\ 0 & \text{otherwise} \end{cases} \tag{13}$$

where τ_R and τ_H are the time constant of dopamine and acetylcholine, $DA(t)$ and $AC(t)$ represents the source of dopamine and acetylcholine due to the activity of dopaminergic neurons and cholinergic neurons. The agent's dopamine concentration increases at time t_{reward} when it completes a single-step movement and arrives within the target range. If the agent fails to find a reward after completing the single-step movement, its acetylcholine concentration rises at time t_{no}.

Table 4
Parameter values of the R-STDP learning rule in the hippocampus and basal ganglia.

Parameter	Context-DG	LC-D1	LC-D2
A_+	1.5	0.1	0.1
A_-	−1.5	−0.1	−0.1
τ_+	10 ms	20 ms	20 ms
τ_-	10 ms	20 ms	20 ms
τ_E	3 ms	1 s	1 s
τ_W	5 s	10 s	10 s
τ_R	80 ms	80 ms	80 ms
τ_H	80 ms	80 ms	80 ms

The plastic connections between contextual neurons and DG facilitate target location learning. When the agent reaches the target, target-encoding DG neurons fire concurrently with dopamine surges. Consequently, synapses between target-representing DG neurons and contextual neurons undergo potentiation, while other DG-contextual connections remain largely unaffected due to rapid eligibility trace decay. As shown in Fig. 2(b), contextual neuron populations develop maximally strengthened connections with $S4_{DG}$.

Since the basal ganglia module needs to process task-dependent distal reward problems [26,42], the basal ganglia module implements an identical R-STDP rule for its LC-D1 and LC-D2 connections (with parameters specified in Table 4). In this circuit, each LC neuron encodes specific egocentric position information, enabling the system to acquire stimulus–response associations. During navigation tasks such as the forward movement task illustrated in Fig. 2(c) (where LC activation progresses sequentially through LC1 to LC4), this learning mechanism produces characteristic synaptic modifications. Active forward-movement D1/D2 neurons establish eligibility traces with co-active LCs, and subsequent reward delivery converts these eligibility traces into connection changes. This mechanism enables reward-driven synaptic updates to be temporally linked to prior decision events, even when there is a significant delay between action execution and reward reception, effectively handling the distal reward challenge within the LC-D1/D2 circuit. Specifically, LC1 develops maximally potentiated connections with D1 neurons, promoting forward action, while forming maximally depressed connections with D2 neurons that suppress forward action. These experience-dependent modifications create enduring position-action biases, such that subsequent encounters with spatial configurations matching LC1's encoded pattern preferentially elicit forward movement responses.

Task performance is evaluated using the number of steps taken by the network to reach the target location. To ensure that early learning episodes could complete successfully, we set a relatively high maximum step threshold (200 steps). This measure reflects navigation efficiency and is used consistently across trials to assess learning progress.

2.4. Real robot experimental platform

On the hardware front, an onboard computer (Raspberry Pi 5, Quad-Core ARM Cortex-A76) manages communication with the host computer. The robot's software architecture is built on the ROS 2 framework, which facilitates information exchange between the mobile platform and the host system. The navigation algorithm itself executes on the host computer. The mobile robot is equipped with four Mecanum wheels, enabling omnidirectional movement via differential speed control of each hub motor. A wheel odometry system collects encoder pulse signals from each wheel, which are then integrated with calibrated wheel diameter parameters and the Mecanum kinematic model to calculate the vehicle's pose in real time. At the beginning of each trial, the robot is manually positioned at the start location and the odometry is zeroed.

Spatial alignment between the neural model and the real-world environment is achieved through a biologically-inspired mapping scheme. The square testing arena is divided into a 15×15 grid, where each grid cell corresponds to the spatial preference field of one place cell (DG, CA3, or CA1). When the robot enters a specific grid cell, the corresponding place cell is activated and emits spikes, effectively grounding the hippocampal spatial representation in physical space.

The same discretization scheme is applied to LC neurons. Landmark positions are predefined in the environment, and when the robot's relative location to a landmark falls within a specified grid region, the corresponding LC neuron fires. This framework establishes a spatiotemporal neural representation that mirrors the geometric structure of the physical world.

3. Results

3.1. Simulation of navigation task

Our model was first tested in an open-field navigation task, with separate simulations conducted for the basal ganglia module and hippocampal module. The environment is modeled as a square arena where the agent could move freely. Each simulation begins with the agent starting from a fixed position on the left side of the arena, with an invisible target located on the right side marked by a visible landmark. It should be noted that the agent has no prior knowledge of the spatial relationship between the target and the landmark. The agent is required to learn to navigate to the target position during the training process.

Action selection in the basal ganglia module was determined by the firing rates of MC neurons. When a neuron's firing rate exceeded the threshold, the corresponding movement direction was selected. Fig. 3(a) shows raster plots of basal ganglia activity,

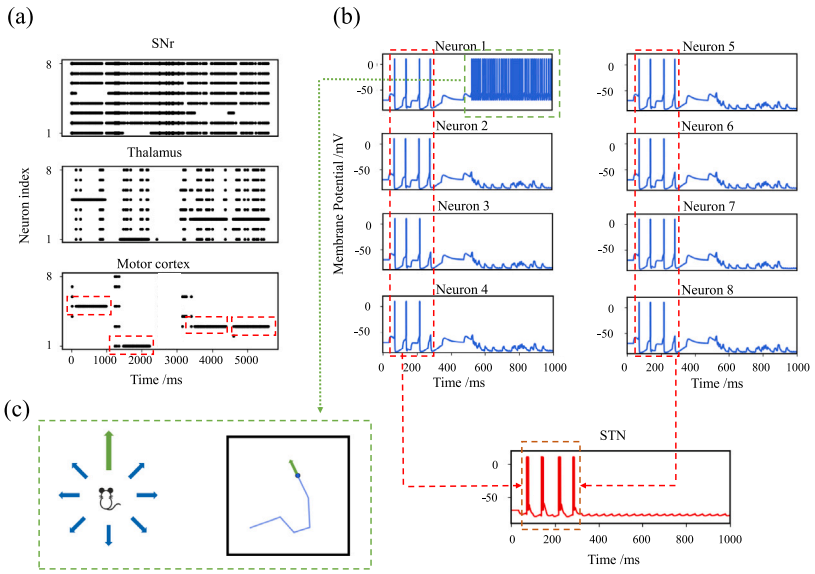

Fig. 3. Schematic illustration of navigation mediated by the basal ganglia module. (a) Raster plots showing spiking activity in SNr, TH, and MC neurons within the basal ganglia network over a 5000 ms period, during which four action selections were made. (b) Demonstration of STN-mediated conflict resolution. Blue lines show membrane potential dynamics of eight MC neurons representing different movement directions. Red line shows corresponding membrane potential changes in STN neurons. (c) Left figure shows action selection among eight possible directions, with the chosen forward movement indicated by the green arrow. Right figure shows environmental trajectory (blue solid line) showing the agent's forward movement relative to its body orientation (green arrow). (For interpretation of the references to color in this figure legend, the reader is referred to the web version of this article.)

where high-frequency firing in MC neurons indicates action selection. The SNr, as the primary output nucleus of the basal ganglia, exerts inhibitory projections to the TH. Since the MC receives excitatory inputs from the thalamus, during action selection the corresponding neurons in TH and MC exhibit similar high-frequency firing patterns, while neurons in the SNr corresponding channel remain in a resting state. (Fig. 3(a)). During action selection, conflicts may arise as demonstrated by the red dashed box in Fig. 3(b). The basal ganglia module initially exhibits concurrent activity in multiple action channels due to similar input patterns, resulting in selection conflicts. This triggered STN activation, which broadly inhibited all MC neurons and temporarily paused action selection to resolve the conflict. After this transient suppression, the BG successfully selected a single action (green dashed box). Fig. 3(c) illustrates the chosen movement (forward motion), with the corresponding trajectory in global coordinates.

During the training process, the agent gradually learns to reach the target area via a relatively short path. Fig. 4(a) compare navigation paths during early and late training stages. Pathlengths to the target progressively shortened, transitioning from random exploration to efficient goal-directed navigation. The corresponding spatial distribution of mean synaptic weights between LCs and striatum D1 neurons undergo dynamic modifications across learning process (Fig. 4(b)). Each square represents the total connection strength for LCs encoding a specific egocentric position. In the initial training phase, the untrained connections between LCs and D1 neurons (Fig. 4(b) left panel) lead to random exploration behavior driven by stochastic inputs. Upon reward discovery, the relevant stimulus-action associations are strengthened through selective modulation of connections between activated LC and specific striatal neurons. As learning progresses, when a landmark appears in particular egocentric positions, the agent develops directional movement preferences that reliably lead to reward. For instance, in well-trained conditions, frontal landmark positions elicit forward movements. The synaptic enhancements are most pronounced for central positions (Fig. 4(b) right panel), reflecting more frequent reward encounters when landmarks are proximal to agent, which demonstrates successfully encoding the reward's consistent spatial relationship to the landmark.

Therefore, the evolution of steps required to find rewards across training epochs shows an overall decreasing trend (Fig. 4(c)). Meanwhile, intermittent increases in step counts reflect the system's maintained exploratory capacity attributed to occasional investigation of alternative paths.

Unlike the basal ganglia navigation module, the hippocampal module acquires spatial environment knowledge through the agent's exploratory behaviors and utilizes the learned environmental information to guide navigation. Fig. 5 illustrates the navigation process governed by the hippocampal module, where the agent begins in the top-left corner of the environment with the target situated at the bottom-right corner (Fig. 5(d)). In the hippocampal navigation experiments, the agent initially engages in random exploration to train the connection weights between CA3-CA1 and DG-CA3 networks, thereby acquiring knowledge of environmental spatial relationships, including connectivity and relative distances between locations. Reward discovery triggers dopamine release, which potentiates connections between DG cells encoding target position and context neurons, thereby completing the hippocampal learning process. Fig. 5(a) presents a schematic diagram of synaptic connections among hippocampus, with corresponding post-learning synaptic weights depicted in Fig. 5(b), where solid circles represent presynaptic neurons. The Context-DG weight matrix in

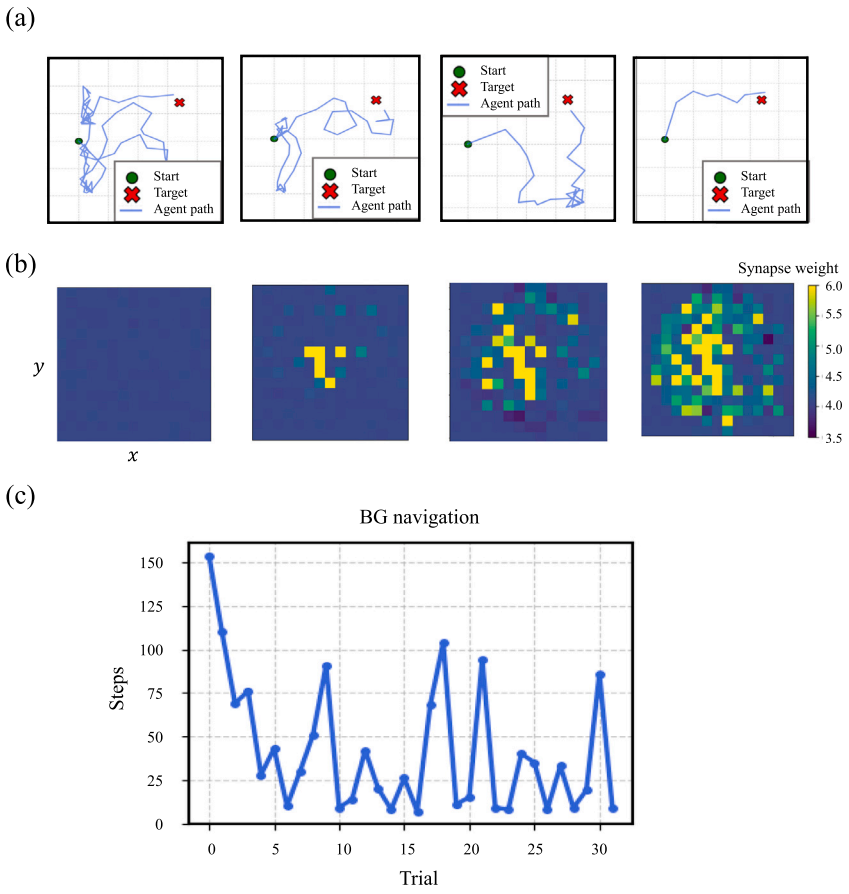

Fig. 4. Navigation performance of the basal ganglia module. (a) Evolution of navigation trajectories across training. Panels from left to right depict the trajectories during: the 1st, 10th, 16th, and 30th training sessions. (b) Spatial distribution of mean feedforward weights from landmark cells to striatal D1 neurons. Panels from left to right depict the weight maps during: the 1st, 10th, 16th, and 30th training sessions. Each square represents the average synaptic weight between a landmark cell and all D1 striatal neurons encoding its preferred location. (c) Training curve showing the number of steps required for the agent to find the reward across sessions.

the top panel of Fig. 5(b) demonstrates strengthened connections between context neurons and DG neurons corresponding to target position. The DG-CA3 weight patterns in the middle panel of Fig. 5(b) exhibit learned proximity relationships to the target, forming a gradient-like profile that implicitly encodes potential navigation paths toward the goal location. The bottom panel of Fig. 5(b) reveals the feedforward CA3-CA1 connection weights, showing potentiated synapses between CA3 neurons encoding the current position and CA1 neurons representing adjacent locations, indicating spatially proximal reachable positions. Fig. 5(c) displays the CA1 neuronal firing pattern that determines movement decisions. The highest firing frequency occurs in CA1 neurons corresponding to the current position, with a progressively decreasing firing rate gradient extending rightward. Through synaptic weight modulation, CA1 firing patterns guide the agent's movement toward the target, which are driven by inputs from context cells and place-specific currents.

Following the learning process described above, the navigation paths generated by the hippocampal module are presented in Fig. 6(a). In the left panel, the agent initially explores the environment randomly from the starting position until eventually discovering the reward. After this initial trial, the navigation path becomes significantly shortened in right panel, enabling faster target acquisition. Unlike the basal ganglia module, the hippocampal module can identify relatively efficient paths after just a single reward discovery trial, demonstrating its reward-sensitive characteristics. However, this capability requires prior environmental exploration to establish an internal spatial model within the hippocampus.

Fig. 6(b) compares the number of steps required to reach the target across training epochs, with and without integration of the hippocampal module. The hippocampal decision outputs provide constant current inputs to stimulate corresponding motor neurons. Therefore, the incorporation of the hippocampal module substantially accelerates the model's training speed, as evidenced by the rapid reduction in navigation steps.

3.2. Simulation of Morris water-maze

We first validated the model's plausibility using the classic Morris water maze paradigm. In this task, rodents swim in opaque water to locate a hidden platform, with a visible landmark maintaining a fixed offset from the platform. Animals underwent training

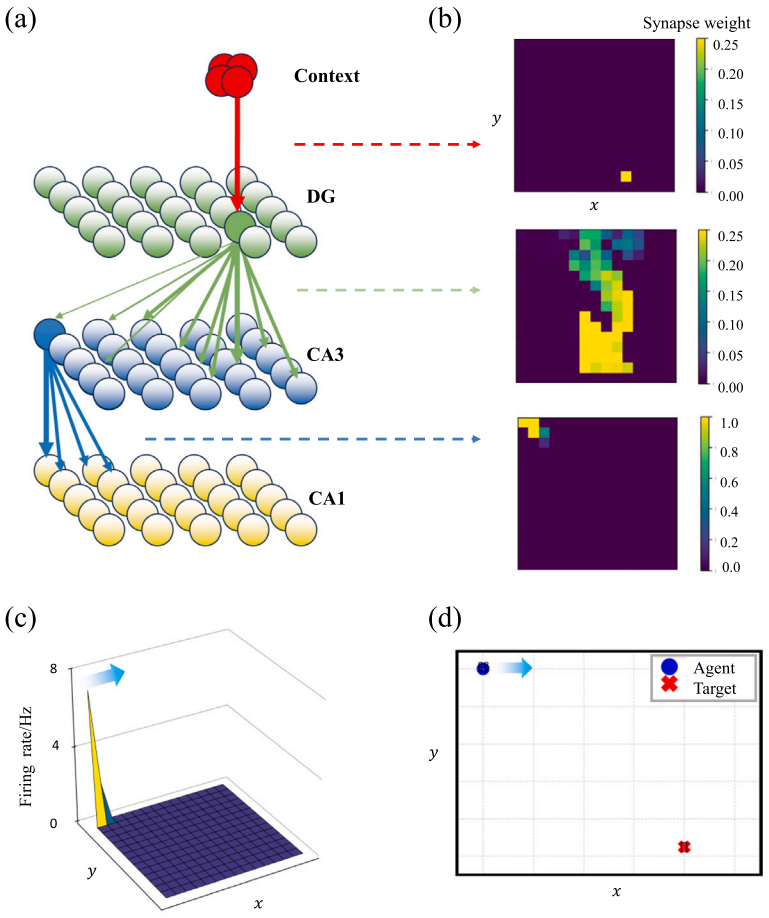

Fig. 5. Hippocampal module navigation schematics. (a) Schematic diagram of synaptic connections between neuronal populations in hippocampus. Solid-colored circles represent presynaptic neurons. (b) Synaptic weight distribution after training. Top panel: mean feedforward connection weights between cortical context neurons and the DG layer. Each grid square represents the average synaptic weight between DG cells encoding a specific spatial position and the 4 context neurons. Mid panel: feedforward weights from DG neurons encoding the target position to CA1 neurons. Bottom panel: feedforward weights from CA3 neurons (encoding the agent's current location at top-left) to CA1 neurons. (c) Spatial firing rate distribution of CA1 neurons. The blue arrow indicates the agent's current movement strategy. (d) Schematic of the agent's current position (top-left) and target location in the environment. (For interpretation of the references to color in this figure legend, the reader is referred to the web version of this article.)

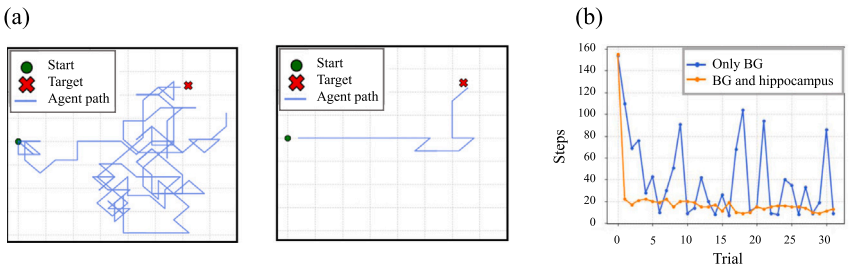

Fig. 6. Navigation results of the hippocampal module. (a) The agent's path from start to terminal points. Left panel: Initial random exploration path of the hippocampal navigation module before learning, showing the first successful target discovery. Right panel: navigation path after learning in the hippocampal module. (b) Comparison of steps required to find rewards across training epochs, demonstrating performance improvement before and after hippocampal module integration.

divided into multiple sessions, each comprising 4 trials. At each session, the spatial configuration of landmarks and target positions varies, with potential locations indicated by red crosses in Fig. 7(a). Physiological data revealed that during initial trials of each session, hippocampally lesioned mice outperformed intact ones. And intact mice exhibited initial wandering near previous target locations due to residual memory. However, lesioned mice showed impaired within-session learning but maintained cross-session

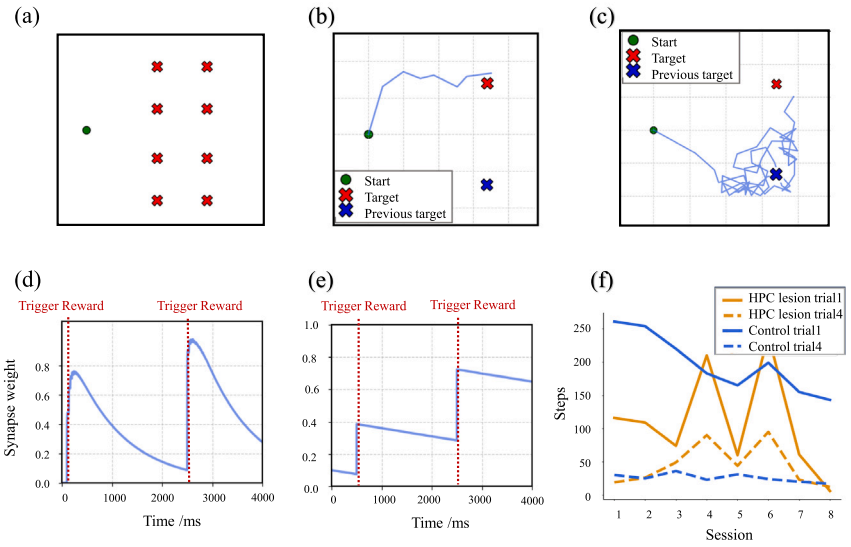

Fig. 7. Morris water maze experimental results. (a) Navigation setup: Starting positions (green circles) and possible target-landmark configurations (red crosses) for each experimental phase. (b) Simulated navigation paths with hippocampal lesioning during target-switching conditions. (c) Simulated navigation paths with intact brain circuitry during target-switching conditions. (d) Temporal dynamics of summed connection weights between context neurons and the DG layer. The red dashed line indicates reward acquisition. (e) Temporal dynamics of mean connection weights between LC and D1 neuronal populations. The red dashed line indicates reward acquisition. (f) Simulation results replicating rodent water maze experiments. Target-landmark positions were changed at each phase initiation (solid lines: first trial of each phase; dashed lines: fourth trial of each phase). (For interpretation of the references to color in this figure legend, the reader is referred to the web version of this article.)

performance unaffected by landmark shifts, suggesting they learned to navigate to targets relative to the landmark's stable egocentric relationship [28].

In our model, phase-wise relocation of the landmark-platform pair forced re-encoding of reward positions in the hippocampus's allocentric system. Conversely, the LCs' egocentric coding preserved learned stimulus–response associations across phases. To simulate target-switching effects on hippocampal processing, we implemented time-dependent decay of context-DG synaptic weights, representing diminishing motivation to revisit obsolete targets when rewards were persistently absent. During phase transitions, hippocampal-lesioned agents (Fig. 7(b)) directly approached new targets via preserved basal ganglia navigation, while intact agents initially wandered near old locations before hippocampal influence attenuated, ultimately redirecting to new targets under basal ganglia control (Fig. 7(c)). The synaptic weights of LC-D1 connections exhibited smaller magnitude changes compared to context-DG connections, demonstrating slower but more stable learning dynamics, a characteristic reflecting the basal ganglia's involvement in habitual action learning (Fig. 7(d) and (e)). Our simulations successfully replicated key experimental findings (Fig. 7(f)): (1) Within-phase superiority of intact models reflected rapid hippocampal learning of environmental contingencies; (2) Cross-phase resilience of lesioned models demonstrated the basal ganglia's stable egocentric strategy when allocentric relationships changed and egocentric relationships remained invariant.

3.3. Simulation of the plus-maze task

The hippocampal-basal ganglia navigation model was further validated using a place/response learning task. In this paradigm, mice were trained to locate food rewards in one arm of a plus-maze, always starting from the same arm while the opposite arm remained blocked [45]. During testing, mice began from the opposite starting position. Their strategy was classified as response learning if they made the same egocentric turn (leading to the opposite arm), as indicated by the orange arrow in Fig. 8(a), or as flexible place learning if they made the opposite turn (reaching the original reward location), as indicated by the green arrow in Fig. 8(a). Our simulations examined the dynamic interplay between hippocampal place learning and basal ganglia response learning.

Physiological studies demonstrated that hippocampal-lesioned mice predominantly adopted response strategies and tended to miss target, as shown in top panel of Fig. 8(b), while striatum-lesioned mice preferred place strategies to locate the target as shown in bottom panel of Fig. 8(b) [46]. Intact animals transitioned from initial place-based to response-based strategies with prolonged training. Our model replicated these findings through selective module inactivation. We simulated the early training phase with 8 trials and the late training phase with 16 trials. Early in training, simulated healthy control agents predominantly followed place strategies (hippocampus-dependent), but shifted to response strategies (basal ganglia-dependent) after extensive training (Fig. 8(d) blue line). Hippocampus-lesioned mice predominantly exhibited a response strategy preference (Fig. 8(d) orange line), while striatum-lesioned mice consistently relied on a place-based strategy (Fig. 8(d) green line). The simulation results are highly consistent with experimental observations.

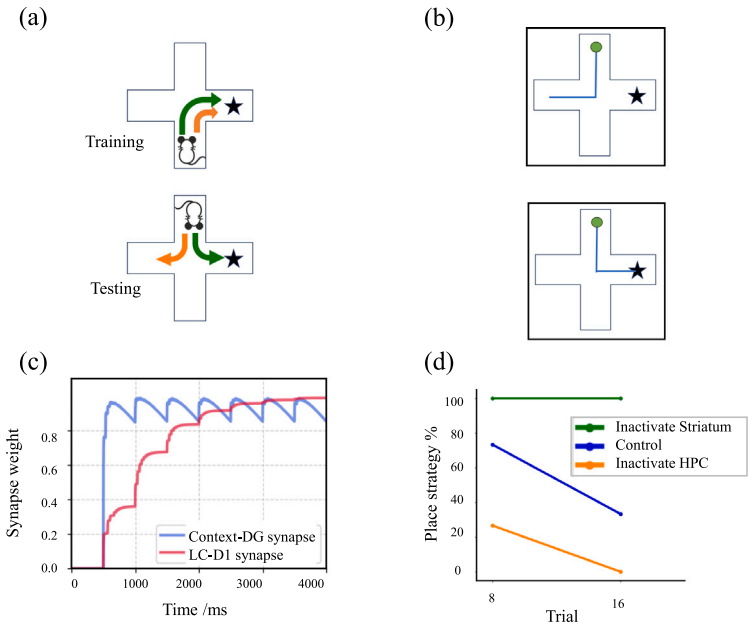

Fig. 8. Plus-maze navigation simulations. (a) Schematic of the cross-maze task. During training, mice started from the south arm to locate rewards; during testing, they started from the north arm. (b) Representative test-phase trajectories. Top panel: striatum-dependent navigation adopting response strategy in hippocampus-lesioned mice. Bottom panel: hippocampus-dependent navigation adopting place strategy in striatum-lesioned mice. (c) Synaptic weight dynamics during training: Blue line: Summed weights between context neurons and DG; Red line: Mean weights between LC and D1 neurons. (d) Percentage of place strategy choices (vs. response strategy) after 8 and 16 training sessions, comparing intact, hippocampus-lesioned, and striatum-lesioned conditions. (For interpretation of the references to color in this figure legend, the reader is referred to the web version of this article.)

This behavioral shift emerged from differential learning rates between systems (Fig. 8(c)). Hippocampal synapses (blue line) reached maximal weights immediately upon first reward discovery, enabling rapid place learning. In contrast, striatal weights (red line) accumulated gradually through reinforced stimulus–response associations. Initially, striatal activity was insufficient to override hippocampal inputs to motor cortex. As LCs-striatum connections strengthened with training, basal ganglia outputs eventually dominated movement selection, reflecting habit formation. This resembles Fabian's simulations showing primates transition from goal-directed to habitual behaviors, confirming our model's biological plausibility in representing navigation strategy shifts [26].

3.4. Real-world reaching target task

We designed a mobile robot reaching target experiment to validate our hippocampal-basal ganglia navigation model in real-world environments. In this experiment, the robot starts from a designated position and trains its navigation trajectory through repeated target-seeking tasks. The testing area is a 2.5 m × 2.5 m square space with both the target and visible landmark located in the upper-left corner.

A mobile robot equipped with odometry and Mecanum-wheeled platform is deployed. An onboard computer (Raspberry Pi 5, Quad-Core ARM Cortex-A76) handles information exchange with the host computer via ROS2-basedframework. The operational flowchart of the autonomous vehicle navigation experiment is illustrated Fig. 9(a). The robot provides real-time positional data to the host computer, which then modulates dopamine or acetylcholine levels based on whether the target is reached, thereby updating synaptic weights. Subsequently, the host computer processes the vehicle's positional information to encode both landmark-egocentric (via LCs) and global-allocentric (via hippocampus) spatial representations. Following network simulation, action decisions are generated based on motor neuron firing patterns, producing movement vectors that are transmitted to the vehicle. After target acquisition, the vehicle resets for subsequent training trials.

The mobile robot initially explores the environment randomly to reach the target, and modulate synaptic weights in model by repeatedly completing the task sequence of target acquisition and return to start point. The movement paths exhibit distinct changes between before and after training. Fig. 9(b) left panel displays the initial exploratory paths during early training phases, showing complex, circuitous routes to the target. After 16 training epochs, the robot develops efficient, direct navigation paths as demonstrated in Fig. 9(b) right panel. The progressive reduction in required movement steps across training sessions indicates successful acquisition of optimal navigation strategies (Fig. 9(c)).

4. Discussion

This paper proposes a navigation dynamics model of hippocampus-basal ganglia coupling, constructed using LIF neurons. The neuronal nuclei in the model are connected with biological plausibility, endowing the model with a certain degree of biological

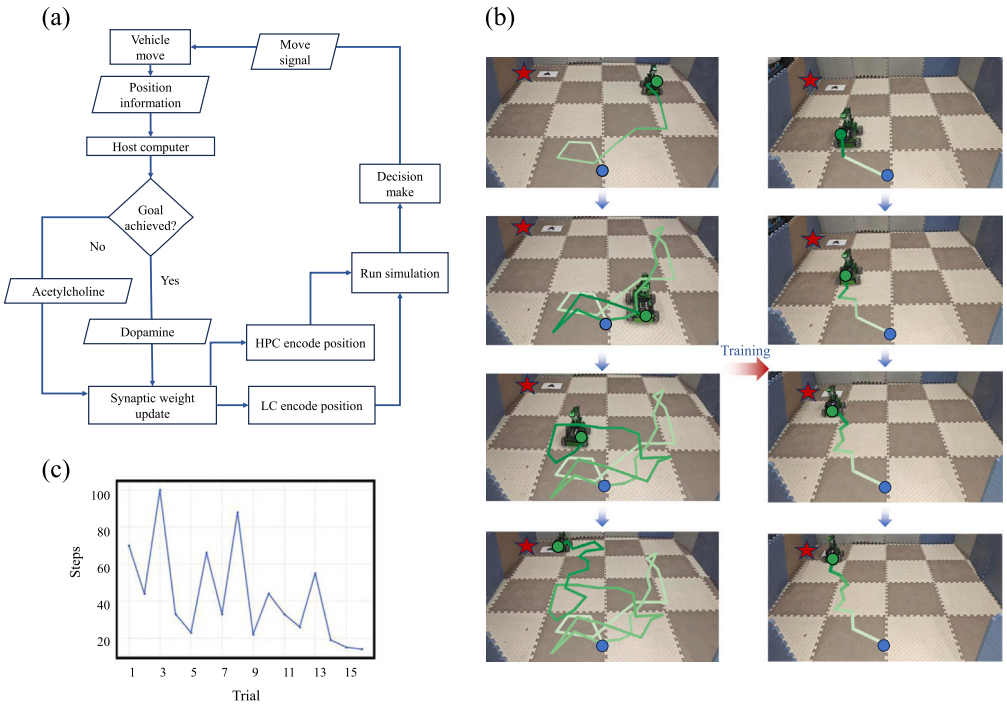

Fig. 9. Mobile robot reaching target experiment. (a) Flowchart of the mobile experiment. (b) The path of the mobile robot from the blue starting point to gradually reach the target has changed before and after training. The trajectory is visualized with a color gradient from light to dark. (c) Number of steps taken by the autonomous vehicle to reach the target as a function of training sessions. (For interpretation of the references to color in this figure legend, the reader is referred to the web version of this article.)

interpretability. The hippocampus and basal ganglia each play distinct functional roles, enabling the learning of spatial environments and stimulus–response associations, ultimately guiding the agent to accomplish navigation tasks.

Our model explores the changes in target-finding paths and learning speeds under navigation strategies driven by the basal ganglia versus the hippocampus. The hippocampus model, which pre-learns the environment, can reach the target faster compared to the model relying solely on the basal ganglia. Subsequently, we used this model to replicate the navigation behaviors of lesioned and healthy mice in the Morris water maze and plus-maze experiments, demonstrating that our model aligns to some extent with the navigation learning mechanisms of mice. Finally, we applied our model to a vehicle target-seeking task, where the vehicle successfully reached the target location via a shorter path, indicating that our model can interact with real-world environments to accomplish training and learning.

Compared to other studies using spiking neural networks (SNNs) to investigate biological navigation [31,32], our model provides a more detailed consideration of the contributions of multiple brain regions—the hippocampus and basal ganglia—to navigation learning behavior and can examine the effects of hippocampal or basal ganglia damage on navigation. Whereas prior SNN-based models tend to abstract away the anatomical specificity of hippocampal-basal ganglia interactions, and traditional RL models often rely on artificial rule-based switching between strategies, our model incorporates biologically plausible microcircuits and enables dynamic transition between hippocampal and striatal control based on intrinsic neural competition. In contrast to abstract functional models of the hippocampus-basal ganglia, our SNN model drives agent navigation through neuronal spiking, offering greater biological interpretability. At the same time, our model avoids introducing credibility arbitration mechanisms such as [4], instead relying on competitive spiking between motor neurons to switch between hippocampus-dominated and basal ganglia-dominated navigation strategies. During training, we observe intermittent increases in the number of steps required to reach the target. This fluctuation is primarily caused by noise affecting the initial action selection, especially when the learned policy is not yet fully stabilized. These fluctuations reflect the model's retained exploratory capacity and are commonly observed in systems balancing exploration and exploitation. Despite its interpretability, our model currently relies on manually defined allocentric (place) and egocentric (landmark) representations as inputs. While this design simplifies the experimental setup and highlights learning dynamics, it limits the autonomy of the agent in perceiving and constructing spatial representations. This abstraction is common in biologically inspired SNN models but prevents end-to-end learning. In future work, we aim to incorporate sensory modules, such as vision or proximity-based encoding, to allow more biologically grounded perception and enable fully autonomous navigation from sensory inputs.

In summary, our research not only provides a biologically plausible hippocampus basal ganglia circuit model capable of realizing biological navigation functions but also offers insights into the model's application in real-world tasks. Currently, our model only

performs navigation tasks in simple, small-scale environments. When the number of neurons encoding position and action increases significantly, the network's operation and training become slower. In future work, we will further explore the model's navigation performance in complex environments and investigate how the hippocampus-basal ganglia structural network can enhance SNN models applied to robotic training.

CRediT authorship contribution statement

Haobin Wei: Writing – original draft, Validation, Supervision, Software, Resources, Project administration, Methodology, Investigation. **Lining Yin:** Writing – review & editing, Visualization. **Songan Hou:** Writing – review & editing, Visualization. **Ying Yu:** Writing – review & editing, Writing – original draft, Validation, Supervision. **Qingyun Wang:** Writing – review & editing, Visualization.

Declaration of competing interest

The authors declare that they have no known competing financial interests or personal relationships that could have appeared to influence the work reported in this paper.

Acknowledgments

This work was supported by the National Natural Science Foundation of China (Grants Nos. 12332004, 12472053, 123B2023, 124B2032) and the Fundamental Research Funds for the Central Universities, China (No. 501QYJC2024105005)

Data availability

Data sharing is not applicable to this article as no new data were created or analyzed in this study.

References

[1] Geva-Sagiv M, Las L, Yovel Y, Ulanovsky N. Spatial cognition in bats and rats: from sensory acquisition to multiscale maps and navigation. Nature Rev Neurosci 2015;16(2):94–108.
[2] Epstein RA, Patai EZ, Julian JB, Spiers HJ. The cognitive map in humans: spatial navigation and beyond. Nature Neurosci 2017;20(11):1504–13.
[3] Wang X, Hou Z-G, Lv F, Tan M, Wang Y. Mobile robots' modular navigation controller using spiking neural networks. Neurocomputing 2014;134:230–8.
[4] Zou Q, Cong M, Liu D, Du Y. A neurobiologically inspired mapping and navigating framework for mobile robots. Neurocomputing 2021;460:181–94.
[5] O'Keefe J, Nadel L. The cognitive map as a hippocampus. Behav Brain Sci 1979;2(4):520–33.
[6] Chersi F, Burgess N. The cognitive architecture of spatial navigation: hippocampal and striatal contributions. Neuron 2015;88(1):64–77.
[7] White NM. The role of stimulus ambiguity and movement in spatial navigation: a multiple memory systems analysis of location discrimination. Neurobiol Learn Mem 2004;82(3):216–29.
[8] O'Keefe J, Dostrovsky J. The hippocampus as a spatial map, preliminary evidence from unit activity in the freely-moving rat. Brain Res 1971;34(1):171–5.
[9] Taube JS, Muller RU, Ranck JB. Head-direction cells recorded from the postsubiculum in freely moving rats, i. description and quantitative analysis. J Neurosci 1990;10(2):420–35.
[10] Hafting T, Fyhn M, Molden S, Moser M-B, Moser EI. Microstructure of a spatial map in the entorhinal cortex. Nat 2005;436(7052):801–6.
[11] Tolman EC. Cognitive maps in rats and men. Psychol Rev 1948;55(4):189.
[12] Yin HH, Knowlton BJ. The role of the basal ganglia in habit formation. Nature Rev Neurosci 2006;7(6):464–76.
[13] Yin HH, Knowlton BJ, Balleine BW. Lesions of dorsolateral striatum preserve outcome expectancy but disrupt habit formation in instrumental learning. Eur J Neurosci 2004;19(1):181–9.
[14] Đorđević J, Milošević M, Šuvak N. Non-linear stochastic model for dopamine cycle. Chaos Solitons Fractals 2023;177:114220.
[15] Wagatsuma H, Yamaguchi Y. Neural dynamics of the cognitive map in the hippocampus. Cogn Neurodyn 2007;1:119–41.
[16] Carr MF, Karlsson MP, Frank LM. Transient slow gamma synchrony underlies hippocampal memory replay. Neuron 2012;75(4):700–13.
[17] Jadhav SP, Kemere C, German PW, Frank LM. Awake hippocampal sharp-wave ripples support spatial memory. Sci 2012;336(6087):1454–8.
[18] Frank LM, Brown EN, Wilson M. Trajectory encoding in the hippocampus and entorhinal cortex. Neuron 2000;27(1):169–78.
[19] Stachenfeld KL, Botvinick MM, Gershman SJ. The hippocampus as a predictive map. Nature Neurosci 2017;20(11):1643–53.
[20] Bono J, Zannone S, Pedrosa V, Clopath C. Learning predictive cognitive maps with spiking neurons during behavior and replays. Elife 2023;12:e80671.
[21] Yan C, Wang R, Qu J, Chen G. Locating and navigation mechanism based on place-cell and grid-cell models. Cogn Neurodyn 2016;10:353–60.
[22] Sarramone L, Fernandez-Leon JA. Grid cell modules coordination improves accuracy and reliability for spatial navigation. Cogn Neurodyn 2025;19(1):1–21.
[23] Srinivasan A, Srinivasan A, Goodman MR, Riceberg JS, Guise KG, Shapiro ML. Hippocampal and medial prefrontal cortex fractal spiking patterns encode episodes and rules. Chaos Solitons Fractals 2023;171:113508.
[24] Mizumori SJ, Puryear CB, Martig AK. Basal ganglia contributions to adaptive navigation. Behav Brain Res 2009;199(1):32–42.
[25] Balleine BW, Dickinson A. Goal-directed instrumental action: contingency and incentive learning and their cortical substrates. Neuropharmacol 1998;37(4–5):407–19.
[26] Chersi F, Mirolli M, Pezzulo G, Baldassarre G. A spiking neuron model of the cortico-basal ganglia circuits for goal-directed and habitual action learning. Neural Netw 2013;41:212–24.
[27] Steele R, Morris R. Delay-dependent impairment of a matching-to-place task with chronic and intrahippocampal infusion of the nmda-antagonist d-ap5. Hippocampus 1999;9(2):118–36.
[28] Morris RG, Garrud P, a. Rawlins J, O'Keefe J. Place navigation impaired in rats with hippocampal lesions. Nat 1982;297(5868):681–3.
[29] Sukumar D, Rengaswamy M, Chakravarthy VS. Modeling the contributions of basal ganglia and hippocampus to spatial navigation using reinforcement learning. PLoS One 2012;7(10):e47467.
[30] Geerts JP, Chersi F, Stachenfeld KL, Burgess N. A general model of hippocampal and dorsal striatal learning and decision making. Proc Natl Acad Sci 2020;117(49):31427–37.

[31] Zannone S, Brzosko Z, Paulsen O, Clopath C. Acetylcholine-modulated plasticity in reward-driven navigation: a computational study. Sci Rep 2018;8(1):9486.
[32] Kumar MG, Tan C, Libedinsky C, Yen S-C, Tan AY. A nonlinear hidden layer enables actor–critic agents to learn multiple paired association navigation. Cerebral Cortex 2022;32(18):3917–36.
[33] Hinman JR, Chapman GW, Hasselmo ME. Neuronal representation of environmental boundaries in egocentric coordinates. Nat Commun 2019;10(1):2772.
[34] Baston C, Ursino M. A biologically inspired computational model of basal ganglia in action selection. Comput Intell Neurosci 2015;2015(1):187417.
[35] Baunez C, Humby T, Eagle DM, Ryan LJ, Dunnett SB, Robbins TW. Effects of stn lesions on simple vs choice reaction time tasks in the rat: preserved motor readiness, but impaired response selection. Eur J Neurosci 2001;13(8):1609–16.
[36] Baunez C, Robbins TW. Bilateral lesions of the subthalamic nucleus induce multiple deficits in an attentional task in rats. Eur J Neurosci 1997;9(10):2086–99.
[37] Ma L, Hyman JM, Durstewitz D, Phillips AG, Seamans JK. A quantitative analysis of context-dependent remapping of medial frontal cortex neurons and ensembles. J Neurosci 2016;36(31):8258–72.
[38] Gönner L, Vitay J, Hamker FH. Predictive place-cell sequences for goal-finding emerge from goal memory and the cognitive map: a computational model. Front Comput Neurosci 2017;11:84.
[39] Amaral D, Lavenex P. Hippocampal neuroanatomy. 2007.
[40] Bi G-q, Poo M-m. Synaptic modifications in cultured hippocampal neurons: dependence on spike timing, synaptic strength, and postsynaptic cell type. J Neurosci 1998;18(24):10464–72.
[41] Hayashi H, Igarashi J. Ltd windows of the stdp learning rule and synaptic connections having a large transmission delay enable robust sequence learning amid background noise. Cogn Neurodyn 2009;3(2):119–30.
[42] Izhikevich EM. Solving the distal reward problem through linkage of stdp and dopamine signaling. Cerebral Cortex 2007;17(10):2443–52.
[43] Florian RV. Reinforcement learning through modulation of spike-timing-dependent synaptic plasticity. Neural Comput 2007;19(6):1468–502.
[44] Matityahu L, Gilin N, Sarpong GA, Atamna Y, Tiroshi L, Tritsch NX, Wickens JR, Goldberg JA. Acetylcholine waves and dopamine release in the striatum. Nat Commun 2023;14(1):6852.
[45] Packard MG, McGaugh JL. Inactivation of hippocampus or caudate nucleus with lidocaine differentially affects expression of place and response learning. Neurobiol Learn Mem 1996;65(1):65–72.
[46] Lee SW, Shimojo S, O'doherty JP. Neural computations underlying arbitration between model-based and model-free learning. Neuron 2014;81(3):687–99.